

# Raman and Infrared-Active Phonons in Hexagonal HoMnO<sub>3</sub> Single Crystals: Magnetic Ordering Effects

A.P. Litvinchuk,<sup>1</sup> M.N. Iliev,<sup>1</sup> V.N. Popov,<sup>2</sup> and M.M. Gospodinov<sup>3</sup>

<sup>1</sup>*Texas Center for Superconductivity and Advanced Materials, and  
Department of Physics, University of Houston, Houston, Texas 77204-5002*

<sup>2</sup>*Faculty of Physics, University of Sofia, 1164 Sofia, Bulgaria and*

<sup>3</sup>*Institute of Solid State Physics, Bulgarian Academy of Sciences, 1184 Sofia, Bulgaria*

(Dated: September 8, 2003)

Polarized Raman scattering and infrared reflection spectra of hexagonal HoMnO<sub>3</sub> single crystals in the temperature range 10-300 K are reported. Group-theoretical analysis is performed and scattering selection rules for the second order scattering processes are presented. Based on the results of lattice dynamics calculations, performed within the shell model, the observed lines in the spectra are assigned to definite lattice vibrations. The magnetic ordering of Mn ions, which occurs below  $T_N=76$  K, is shown to effect both Raman- and infrared-active phonons, which modulate Mn-O-Mn bonds and, consequently, Mn exchange interaction.

PACS numbers: 63.20.Dj, 78.30.-j, 63.20.Ls, 75.47.Lx

## INTRODUCTION

The hexagonal  $RMnO_3$  [ $R = \text{Ho, Er, Tm, Yb, Lu, Y}$ ; space group  $P6_3cm(C_{6v}^3)$ ,  $Z = 6$ ] compounds belong to the class of ferroelectromagnet materials characterized by the coexistence of antiferromagnetic (AFM) and ferroelectric (FE) orderings [1]. The FE and AFM transitions are well separated in temperature with Curie and Néel temperatures being  $T_C > 800$  K and  $T_N \approx 76$  K, and only weak coupling of the two respective order parameters is expected. Such coupling do exist in  $RMnO_3$  materials. For  $YMnO_3$ , for instance, anomalies in the dielectric constant and loss tangent near  $T_N$  [2] and an additional antiferromagnetic contribution to the non-linear optical polarizability below  $T_N$  [3, 4, 5] were found experimentally. Furthermore, a number of magnetic transitions at lower temperatures (below  $T_N$ ) were established for HoMnO<sub>3</sub> due to both Mn in- $xy$ -plane and Ho  $z$ -axis ordering[6, 7]. The Raman scattering is also determined by non-linear terms of polarizability, which may be affected by AFM-FE and/or spin-phonon couplings. In the case of strong couplings the Raman spectra should exhibit anomalies at magnetic transition temperatures. Anomalous Raman scattering due to two-magnon processes was recently reported for  $YMnO_3$ [8], but not confirmed in more recent studies [9, 10]. All these facts give a motivation for a more thorough study of lattice vibrations of hexagonal manganites as a function of temperature through Raman scattering and infrared spectroscopies.

In this paper we report the polarized Raman and infrared reflection spectra of HoMnO<sub>3</sub> single crystals in a broad temperature range. Pronounced phonon anomalies, that are related to spin-phonon or AFM-FE couplings, are observed experimentally. A comparison to the mode frequencies predicted by lattice dynamical calculations (LDA) allowed assignment of the Raman and infrared lines to definite phonon modes or two-phonon Ra-

man scattering processes. No evidence for two-magnon scattering was found in the low temperature antiferromagnetic phase.

## SAMPLES AND EXPERIMENTAL

Pure polycrystalline hexagonal HoMnO<sub>3</sub> was synthesized by a solid-state reaction of stoichiometric amounts of Ho<sub>2</sub>O<sub>3</sub> (99.99%) and MnO<sub>2</sub> (99.99%), and further annealed for 24h at 1120°C in oxygen atmosphere. HoMnO<sub>3</sub> single crystals were grown by High Temperature Solution Growth Method using PbF<sub>2</sub>/PbO/B<sub>2</sub>O<sub>3</sub> flux (PbF<sub>2</sub> : PbO : B<sub>2</sub>O<sub>3</sub> = 0.8 : 0.195 : 0.005). The flux was mixed with HoMnO<sub>3</sub> powder in a 7 : 1 ratio) and annealed in a platinum crucible at 1250°C for 48h in oxygen. After that the temperature was decreased down to 1000°C at a rate of 0.5 C/h. The flux was decanted and well-shaped hexagonal plate-like crystals of typical size  $3 \times 5 \times 0.2$  mm removed from the bottom of the crucible.

The Raman spectra were measured under a microscope using a HR640 spectrometer equipped with a liquid-nitrogen-cooled CCD detector. The 514.5 nm and 632.8 nm lines of Ar<sup>+</sup> and He-Ne laser were used for excitation. The infrared reflectance was measured with a Bomem DA8 Fourier-Transform interferometer equipped with a near-normal incidence reflectance stage and a liquid-helium-cooled bolometer. The real and imaginary parts of dielectric function,  $\epsilon_1(\omega)$  and  $\epsilon_2(\omega)$ , were obtained through Kramers-Kronig analysis.

The lattice dynamical calculations for HoMnO<sub>3</sub> were performed within the shell model used earlier for  $YMnO_3$ [11]. The lattice parameters and atomic positions were taken from Ref.[7].

## RESULTS AND DISCUSSION

## Room temperature data

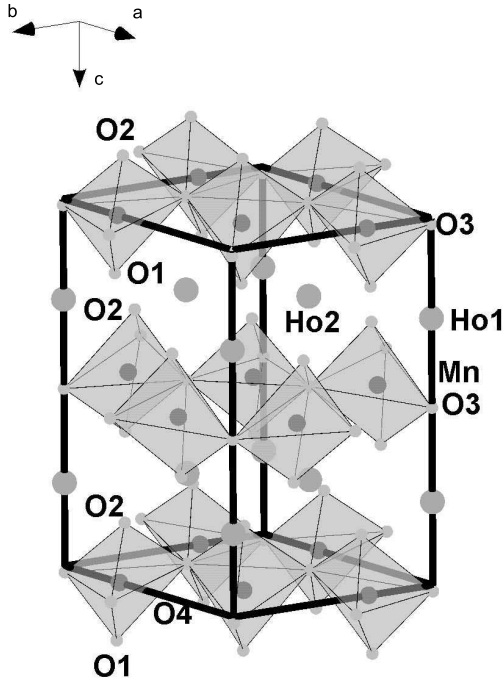


FIG. 1: Crystallographic structure of hexagonal  $\text{HoMnO}_3$  (after parameters of Ref.[7]).

As the crystals are non-centrosymmetric, the modes of  $A_1$  and  $E_1$  symmetry are also infrared active and modulate the dipole moment along the  $z$ -axis and within the  $xy$ -plane, respectively. Optical reflection spectra from the large  $xy$ -plane surfaces correspond to the case when incident and reflected light propagate along the  $z$ -axis and are polarized in the  $(xy)$  plane ( $\vec{E} \perp z$ ). As a consequence,  $E_1$  but not  $A_1$  phonons are accessible in this experimental configuration.

Fig. 2 shows the polarized Raman spectra of  $\text{HoMnO}_3$  at room temperature obtained with two different excitation wavelengths. The most intense spectral feature in both cases is the high-frequency line at  $685 \text{ cm}^{-1}$ , which corresponds to the  $z$ -axis apical oxygen ( $O_1, O_2$ ) vibrations around the Mn ions. It is obvious that the relative line intensities depend strongly on the laser excitation energy. In particular, the line at  $136 \text{ cm}^{-1}$  is not observed in the spectra taken with  $1.96 \text{ eV}$  ( $\lambda_{exc} = 632.8 \text{ nm}$ ) excitation. Another striking feature is the relative intensity variation of the  $685 \text{ cm}^{-1}$  mode taken in  $(zz)$  and  $(xx)$  scattering configuration: for  $\lambda_{exc} = 514.5 \text{ nm}$  the line intensity in  $(zz)$  polarization is by factor of 10 stronger compared to  $(xx)$ , while these lines are similar

The elementary cell of hexagonal  $\text{RMnO}_3$  (space group  $P6_3cm$ ,  $C_{6v}^3$ ,  $Z=6$ ) is shown in Fig. 1. The group-theoretical analysis shows that long-wavelengths zone-center ( $\Gamma$ -point) phonons are distributed among irreducible representations of the  $C_{6v}$  point group as follows[11]:

$$\Gamma_{tot} = 10A_1 + 5A_2 + 10B_1 + 5B_2 + 15E_1 + 15E_2.$$

Of them acoustic, Raman-active and infrared-active phonons are, respectively

$$\Gamma_{ac} = A_1 + E_1;$$

$$\Gamma_R = 9A_1 + 14E_1 + 15E_2;$$

$$\Gamma_{IR} = 9A_1 + 14E_1.$$

Optical modes of  $A_2, B_1,$  and  $B_2$  symmetries are silent.  $A_1$  vibrations correspond to ion displacements along the  $z$  axis. Depending on the scattering configuration one can activate either longitudinal optical (LO)  $A_1$  modes, when phonon propagation direction coincides with the direction of ion displacements ( $z(xx)\bar{z}$  polarization) or transverse (TO) modes ( $y(xx)\bar{y}$  and  $y(zz)\bar{y}$  configurations). Non-polar  $E_2$  vibrations are allowed in  $z(xy)\bar{z}$  polarization, while  $E_1$  are Raman active in  $y(zx)\bar{y}$  polarization. In the latter case experimentally observed  $E_1$  modes have the transverse character.

in intensity under  $\lambda_{exc} = 632.8 \text{ nm}$ . All these facts indicate strong resonant contribution to the Raman scattering spectra, which occurs when incident or scattered light energies are in resonance with a real electronic transition in the material under investigation. Indeed, for  $\text{HoMnO}_3$  a polarized ( $\vec{E} \perp z$ ) on-side Mn  $d-d$  transition near  $1.7 \text{ eV}$  dominates the absorption spectrum in the visible spectral range[12, 13], similar to the case of  $\text{LuMnO}_3$ [14].

In Fig. 3 reflection spectra are shown along with the imaginary part dielectric function  $\epsilon_2(\omega)$  and the loss function  $\text{Im}(-1/\epsilon)$ , maxima of which yield the position of the transverse and longitudinal excitations, respectively. The experimental and theoretical values of the  $\Gamma$ -point mode frequencies are summarized in Tables I and II. Similar to the case of isostructural  $\text{YMnO}_3$  compound[11], more than half of the expected phonons of  $\text{HoMnO}_3$  are observed experimentally and assigned to definite lattice modes. Comparison of mode frequencies of  $\text{YMnO}_3$  (Table IV of Ref.[11]) and  $\text{HoMnO}_3$  (Table I and II) shows their close similarity. We also mention that in the case of  $E_1$ -symmetry modes, which are both Raman and infrared active, the experimentally observed TO frequencies of  $\text{HoMnO}_3$  are in very good agreement (Table II).

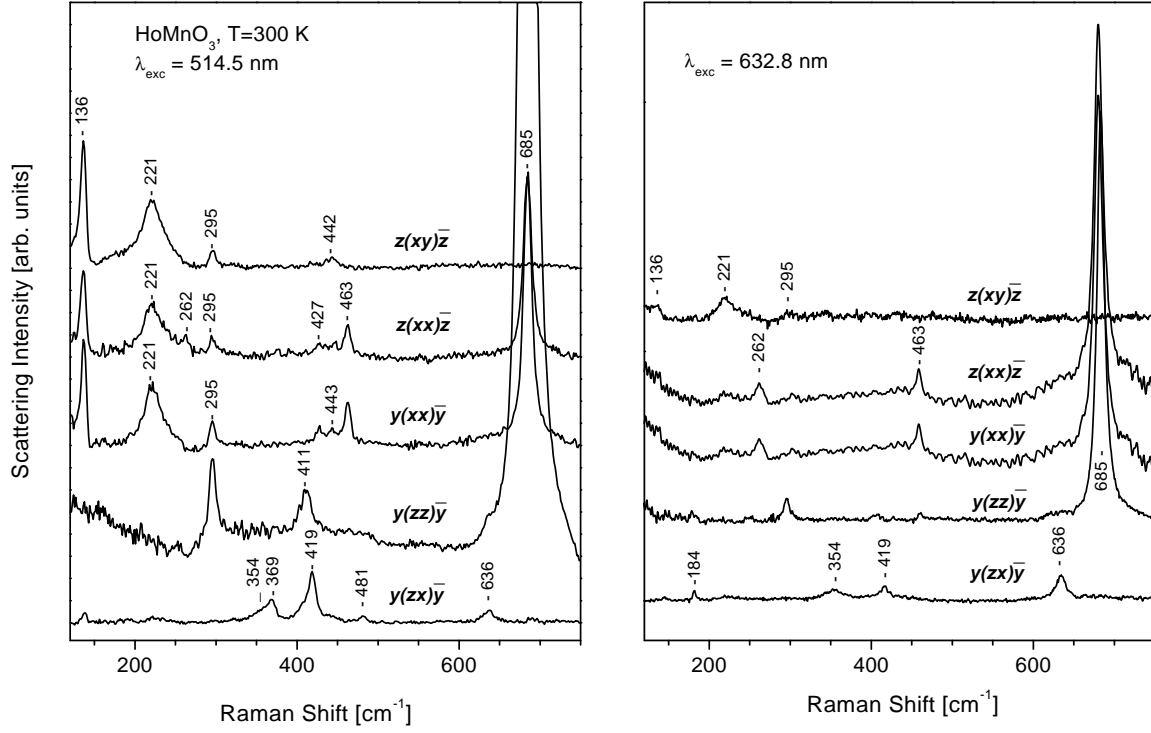


FIG. 2: Room temperature polarized Raman scattering spectra of hexagonal  $\text{HoMnO}_3$  crystals for excitation wavelengths  $\lambda_{\text{exc}} = 514.5$  nm (left panel) and  $632.8$  nm (right panel). According to the selection rules, the spectra correspond to the following symmetries (from top to bottom):  $E_2$ ,  $A_1(\text{LO})+E_2$ ,  $A_1(\text{TO})+E_2$ ,  $A_1(\text{TO})$ , and  $E_1(\text{TO})$ .

TABLE I: Calculated and experimentally observed at 300K in Raman spectra  $A_1$  and  $E_2$  symmetry  $\Gamma$ -point phonon frequencies of hexagonal  $\text{HoMnO}_3$ . All values are given in  $\text{cm}^{-1}$ .

Mode	Theory (TO/LO)	Experiment Raman (TO/LO)	Direction and sign of the largest atomic displacements
$A_1$	125/127		$+z(\text{Ho}/\text{Y1})-z(\text{Ho}/\text{Y2})$
$A_1$	195/234		$\text{rot}_{xy}(\text{MnO}_5)$
$A_1$	245/270	262/262	$+z(\text{Ho}/\text{Y1},\text{Ho}/\text{Y2})-z(\text{Mn})$
$A_1$	291/295	295/295	$x(\text{Mn}),z(\text{O3})$
$A_1$	404/428	411/-	$+z(\text{O3})-z(\text{O4})+x, y(\text{O2})-x, y(\text{O1})$
$A_1$	430/460	427/427	$+z(\text{O4},\text{O3})-z(\text{Mn})$
$A_1$	468/474	463/463	$+x, y(\text{O1},\text{O2})-x, y(\text{Mn})$
$A_1$	598/614		$+z(\text{O1},\text{O2})-z(\text{Mn})$
$A_1$	673/673	685/685	$+z(\text{O1})-z(\text{O2})$
$E_2$	64		$x, y(\text{Ho}/\text{Y1},\text{Ho}/\text{Y2},\text{Mn})$
$E_2$	96		$+x, y(\text{Mn},\text{O3},\text{O4})-x, y(\text{Ho}/\text{Y1},\text{Ho}/\text{Y2})$
$E_2$	137	136	$+x, y(\text{Ho}/\text{Y1})-x, y(\text{Ho}/\text{Y2})$
$E_2$	152		$+x, y(\text{Ho}/\text{Y2})-x, y(\text{Ho}/\text{Y1})$
$E_2$	231	221	$+x, y(\text{O2},\text{Mn})-x, y(\text{O1},\text{O3})$
$E_2$	254		$z(\text{Mn},\text{O2},\text{O1})$
$E_2$	265		$z(\text{Mn},\text{O1},\text{O2})$
$E_2$	330	295	$+z(\text{O2})-z(\text{O1}),x, y(\text{O4})$
$E_2$	339		$+x, y(\text{O1},\text{O2},\text{O4},\text{O3})-x, y(\text{Mn})$
$E_2$	402		$+x, y(\text{O1},\text{O4})-x, y(\text{O2},\text{Mn})$
$E_2$	468	442	$+x, y(\text{O4})-x, y(\text{O1},\text{Mn})$
$E_2$	523		$+x, y(\text{O4},\text{O3})+x, y(\text{O1},\text{O2})$
$E_2$	557		$x, y(\text{O4})$
$E_2$	583		$x, y(\text{O4},\text{O3})$
$E_2$	649		$x, y(\text{O3},\text{O4})$

TABLE II: Calculated and experimentally observed at 300K  $E_1$  symmetry  $\Gamma$ -point phonon frequencies of hexagonal  $\text{HoMnO}_3$ . All values are given in  $\text{cm}^{-1}$ .

Mode	Theory TO/LO	Experiment		Direction and sign of the largest atomic displacements
		IR (TO/LO)	Raman (TO)	
$E_1$	107/110			$+x, y(\text{Mn}, \text{O}3, \text{O}4) - x, y(\text{Ho}/\text{Y}1, \text{Ho}/\text{Y}2)$
$E_1$	143/143	136/146		$+x, y(\text{Ho}/\text{Y}1) - x, y(\text{Ho}/\text{Y}2)$
$E_1$	149/149	160/164		$+x, y(\text{Ho}/\text{Y}2) - x, y(\text{Ho}/\text{Y}1)$
$E_1$	231/231			$+x, y(\text{O}1, \text{O}2) - x, y(\text{Ho}/\text{Y}1, \text{Ho}/\text{Y}2)$
$E_1$	247/253	230/278		$x, y(\text{Mn}, \text{O}3), z(\text{O}1, \text{O}2)$
$E_1$	262/336	289/301		$+x, y(\text{O}1, \text{O}2) - x, y(\text{O}3)$
$E_1$	337/358	303/326		$+x, y(\text{O}1, \text{O}2, \text{O}3) - x, y(\text{O}4, \text{Mn})$
$E_1$	359/397	355/357	354	$+x, y(\text{O}1) - x, y(\text{O}2)$
$E_1$	398/410	369/410	369	$+x, y(\text{O}1) - x, y(\text{O}2)$
$E_1$	471/491	418/476	419	$+x, y(\text{O}4, \text{O}3) - x, y(\text{O}2, \text{O}1, \text{Mn})$
$E_1$	497/537	479/551	480	$+x, y(\text{O}4, \text{O}3, \text{O}1, \text{O}2) - x, y(\text{Mn})$
$E_1$	568/571			$x, y(\text{O}4)$
$E_1$	585/586	593/601		$x, y(\text{O}3)$
$E_1$	648/648		636	$x, y(\text{O}3) - x, y(\text{O}4)$

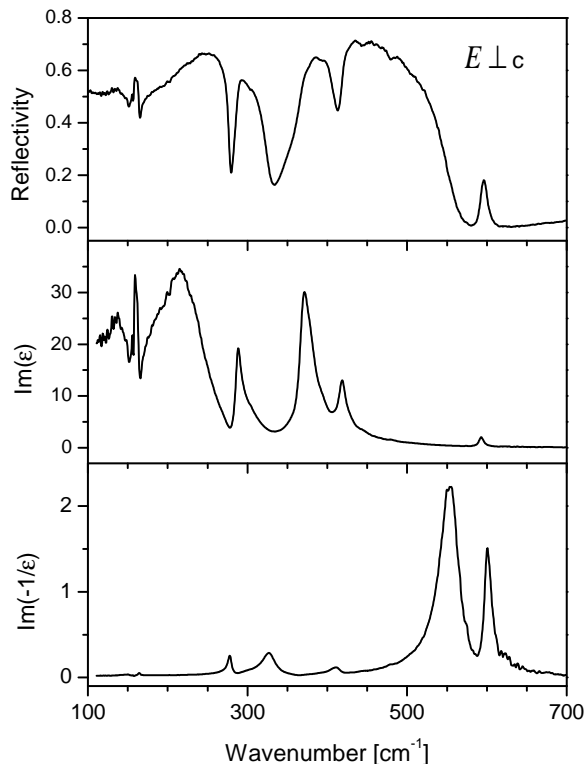


FIG. 3: Spectral dependence of reflectivity (a),  $\text{Im}(\epsilon)$  (b) and the loss function (c) of  $\text{HoMnO}_3$  single crystals for  $\vec{E} \perp z$ (a) at  $T=300$  K.

### Temperature-dependent Raman and infrared spectra

As far as the temperature dependence of Raman active phonon parameters is concerned, most of the phonons exhibit standard anharmonicity-related frequency hardening and linewidth narrowing upon decreasing temperature, proving the absence of any major structural transitions in  $\text{HoMnO}_3$  below 300 K. One of the Raman-active  $E_2$ -symmetry phonons is, however, strongly effected by the antiferromagnetic ordering of Mn ions within  $xy$ -plane below  $T_N$ . As it is seen from the inset in Fig. 4, its frequency deviates from the dependence expected for the anharmonic decay and hardens by as much as  $5 \text{ cm}^{-1}$  between  $T_N$  and 10 K. According to the lattice dynamics calculations (Table I) this phonon corresponds to the rotations of the  $\text{MnO}_5$  structural units in the  $xy$ -plane and effectively modulates Mn-O-Mn exchange interaction. Similar phonon frequency anomalies at the magnetic ordering temperature have been observed earlier in  $\text{CuO}$ [15],  $\text{SrRuO}_3$ [16], and  $\text{CrO}_2$ [17, 18].

Another unusual feature, which we noticed in the temperature-dependent Raman spectra of  $\text{HoMnO}_3$ , is a monotonous intensity increase (by factor of about three) upon cooling from 300K to 10K of the  $A_1$ -symmetry line at  $685 \text{ cm}^{-1}$  in the  $(xx)$  scattering configuration. It may, at least in part, be due to the temperature-induced shift

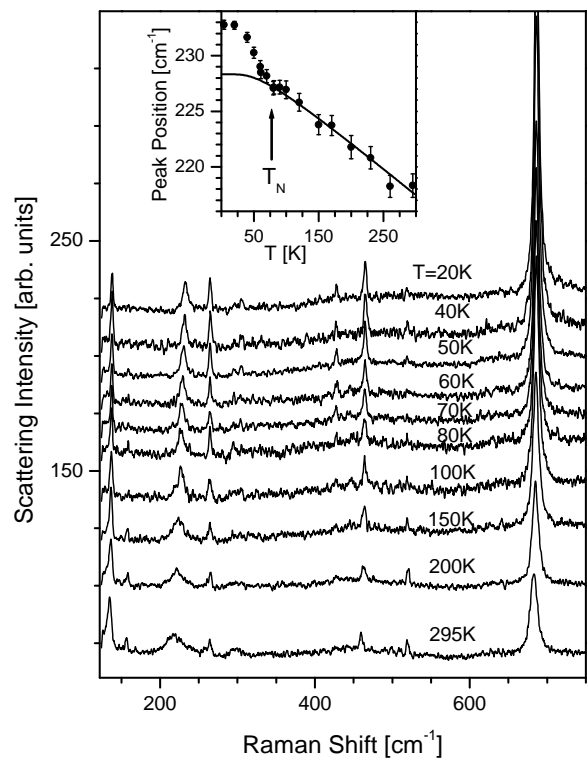


FIG. 4: Raman scattering spectra of  $\text{HoMnO}_3$  in  $z(xx)\bar{z}$  polarization for various temperatures between 20 and 295 K and  $\lambda_{exc} = 514.5 \text{ nm}$ . The inset shows the position of the  $\text{MnO}_5$   $xy$ -rotation mode versus temperature. The solid line shows the peak position expected for a standard anharmonicity-related phonon decay.  $T_N$  marks the Néel temperature.

toward higher energies of the on-side Mn  $d-d$  transition by about  $0.19 \text{ eV}$ [13], which affects the resonant conditions.

The spectral dependence of the imaginary part of  $\text{HoMnO}_3$  dielectric function is shown in Fig. 5 for several temperatures between 10 and 300 K. Here, like for the Raman-active modes, one of the modes exhibits remarkable frequency hardening upon entering the antiferromagnetic state. This  $E_1$ -symmetry mode, centered at  $230 \text{ cm}^{-1}$  at room temperature, corresponds primarily to the in- $(xy)$ -plane Mn-O<sub>3</sub> bond modulation. Recently similar unusual behavior of low frequency phonon  $E_1$  modes was observed in isostructural hexagonal  $\text{LuMnO}_3$  single crystals, suggesting their coupling to the spin system[14]. Several very narrow lines (the full width at half maximum as low as  $3 \text{ cm}^{-1}$ ), which become especially pronounced at lower temperatures at around  $160 \text{ cm}^{-1}$  and  $240 \text{ cm}^{-1}$ , are related to the transitions between 11 levels of  $\text{Ho}^{3+}$  ground multiplet of  $^5I_8$  symmetry, splitted by the crystalline electric field. These transitions, as well as those between ground and excited states, will be discussed in details in a separate publication[13].

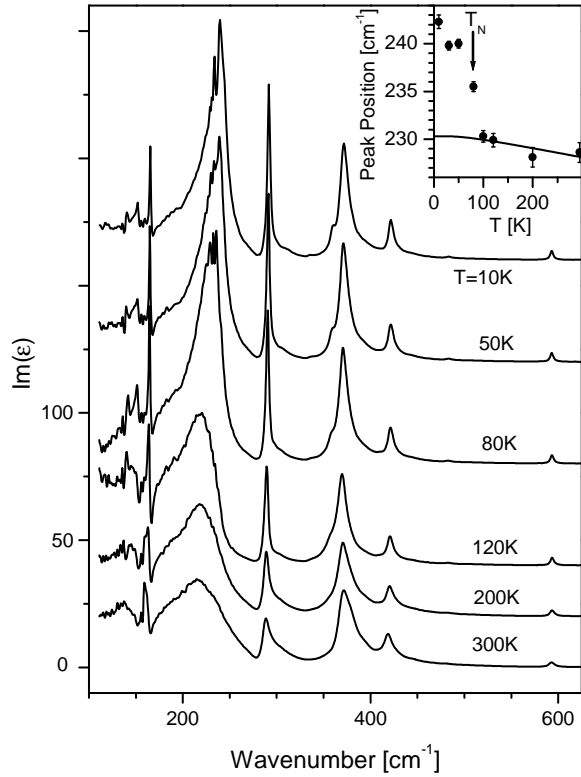


FIG. 5: Temperature dependence of  $\text{Im}(\epsilon)$  for  $\text{HoMnO}_3$  single crystals ( $\vec{E} \perp z$ ). The spectra are displaced vertically for clarity. The inset shows the peak position of a low-frequency mode, which exhibits anomalous hardening below the Néel temperature  $T_N$ . The solid line is a behavior expected for a standard anharmonicity-related shift.

### Second order Raman scattering spectra and group-theoretical selection rules

Unlike the first-order scattering, which due to momentum conservation probes only zone-center ( $\Gamma$ -point) vibrations, the second order scattering involves phonon throughout the entire Brillouin zone. Scattering intensity is governed in this latter case by the scattering selection rules and also phonon density of state, which is determined by the phonon dispersion.

The distribution of all 90 normal vibrations of hexagonal  $\text{HoMnO}_3$  according to the symmetry type at various points of the Brillouin zone (see, e.g. [19]) is summarized in Table III. In this Table special points are grouped according to their symmetry. In Table IV the selection rules for overtones and combination tones are presented for the hexagonal Brillouin zone, where the notations of Refs. [20, 21] are used. It follows from the Table that for all special points of the Brillouin zone overtones always contributes to the fully symmetric  $A_1$  component, while combinations of phonons belonging to different symmetries never contain  $A_1$  representation.

The second-order scattering spectra of  $\text{HoMnO}_3$  single

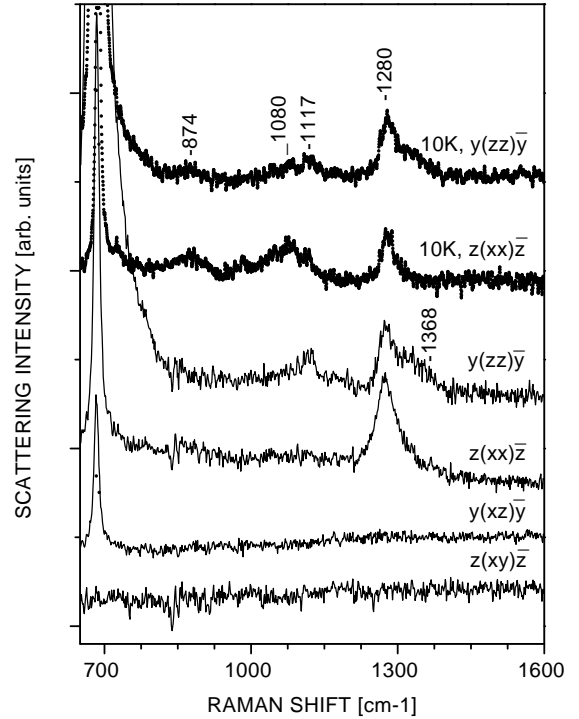


FIG. 6: Second-order polarized Raman scattering spectra of  $\text{HoMnO}_3$  for  $\lambda_{exc} = 514.5$  nm. Two upper spectra are taken at  $T=10\text{K}$ , and the lower four at  $300\text{K}$ .

crystals in various scattering configurations and temperatures 300 and 10K are displayed in Fig. 6. As it is seen, no second-order lines are detected in the spectra obtained for  $(xy)$  and  $(xz)$  polarizations (two lowest curves in Fig. 6). The cut-off frequency of the two-phonon spectrum is expected to be at the double frequency of the highest energy  $\Gamma$ -point phonon ( $2 \times 685 \text{ cm}^{-1} = 1370 \text{ cm}^{-1}$ ). The peak at  $1368 \text{ cm}^{-1}$ , which is observed in the  $(xx)$  polarization, corresponds to the overtone of the highest frequency  $A_1$ -symmetry phonon at the Brillouin zone center. The peak at lower frequency,  $1280 \text{ cm}^{-1}$ , which is observed in both  $(xx)$  and  $(zz)$  scattering geometries, is probably due to the overtone of the same vibration in other special points (K, M, or L). Under this assumption the estimated dispersion of the high-frequency branch through the Brillouin zone is approximately  $45 \text{ cm}^{-1}$ .

Several peaks in the frequency range 1080-1117, which are especially pronounced in the  $(xx)$  polarization at 10K, are probably due to combinations of the high-frequency mode with the phonon branches in the range  $350\text{-}463 \text{ cm}^{-1}$  at various points of the Brillouin zone. A broad peak centered at  $874 \text{ cm}^{-1}$  may be related to the overtones of these latter modes.

We note that the second-order Raman scattering spectra for hexagonal  $\text{HoMnO}_3$  are very similar to those reported earlier for  $\text{YMnO}_3$  in terms of relative line intensities and position of the most intense features[9].

TABLE III: Group-theoretical selection rules for two-phonon scattering processes in hexagonal HoMnO<sub>3</sub>.

Special points and physically irreducible representations	Overtones	Combinations
$\Gamma (C_{6v})$ $\Gamma_1, \Gamma_2, \Gamma_3, \Gamma_4, \Gamma_5, \Gamma_6$	$[\Gamma_1]^2, [\Gamma_2]^2, [\Gamma_3]^2, [\Gamma_4]^2 \supset A_1$ $[\Gamma_5]^2, [\Gamma_6]^2 \supset A_1, E_2$	$\Gamma_1 \times \Gamma_1, \Gamma_2 \times \Gamma_2, \Gamma_3 \times \Gamma_3, \Gamma_4 \times \Gamma_4, \supset A_1$ $\Gamma_1 \times \Gamma_5, \Gamma_2 \times \Gamma_5, \Gamma_3 \times \Gamma_6, \Gamma_4 \times \Gamma_6, \Gamma_5 \times \Gamma_6 \supset E_1$ $\Gamma_1 \times \Gamma_6, \Gamma_2 \times \Gamma_6, \Gamma_3 \times \Gamma_5, \Gamma_4 \times \Gamma_5 \supset E_2$
A ( $C_{6v}$ ) $A_I = A_1 + A_3$ $A_{II} = A_5 + A_6$ $A_{III} = A_2 + A_4$	$[A_I]^2, [A_{III}]^2 \supset A_1$ $[A_{II}]^2 \supset A_1, E_1, E_2$	$A_{III} \times A_{III} \supset A_1$ $A_{II} \times A_{II} \supset A_1, E_1, E_2$ $A_{II} \times A_{III} \supset E_1, E_2$
K ( $C_{3v}$ ) $A_1 + B_1 \rightarrow K_1$ $A_2 + B_2 \rightarrow K_2$ $E_1 + E_2 \rightarrow K_3$	$[K_1]^2, [K_2]^2 \supset A_1$ $[K_3]^2 \supset A_1, E_1, E_2$	$K_1 \times K_1, K_2 \times K_2 \supset A_1$ $K_3 \times K_3 \supset A_1, E_1, E_2$ $K_1 \times K_3, K_2 \times K_3 \supset E_1, E_2$
M ( $C_{2v}$ ) $M_1, M_2, M_3, M_4$	$[M_i]^2 \supset A_1, E_2$	$M_i \times M_i \supset A_1, E_2$ $M_1 \times M_2, M_3 \times M_4 \supset E_2$ $M_1 \times M_3, M_1 \times M_4, M_2 \times M_3, M_2 \times M_4 \supset E_1$
L ( $C_{2v}$ ) $L_I = L_1 + L_3$ $L_{II} = L_2 + L_4$	$[L_I]^2, [L_{II}]^2 \supset A_1, E_1, E_2$	$L_I \times L_I, L_{II} \times L_{II} \supset A_1, E_1, E_2$ $L_I \times L_{II} \supset E_1, E_2$

TABLE IV: Normal vibrations of HoMnO<sub>3</sub> at special points of the hexagonal Brillouin zone.

Point of the Brillouin zone (symmetry)	Irreducible representations
$\Gamma (C_{6v})$	$5(2\Gamma_1 + \Gamma_2 + 2\Gamma_3 + \Gamma_4 + 3\Gamma_5 + 3\Gamma_6)$
$\Delta (C_{6v})$	$5(2\Delta_1 + \Delta_2 + 2\Delta_3 + \Delta_4 + 3\Delta_5 + 3\Delta_6)$
A ( $C_{6v}$ )	$5(2A_1 + A_2 + 2A_3 + A_4 + 3A_5 + 3A_6)$
K ( $C_{3v}$ )	$10(2K_1 + K_2 + 3K_3)$
P ( $C_{3v}$ )	$10(2P_1 + P_2 + 3P_3)$
H ( $C_{3v}$ )	$10(2H_1 + H_2 + 3H_3)$
M ( $C_{2v}$ )	$5(5M_1 + 4M_2 + 5M_3 + 4M_4)$
U ( $C_{2v}$ )	$5(5U_1 + 4U_2 + 5U_3 + 4U_4)$
L ( $C_{2v}$ )	$5(5L_1 + 4L_2 + 5L_3 + 4L_4)$
$\Sigma (C_s^d)$	$45(\Sigma_1 + \Sigma_2)$
F ( $C_s^d$ )	$45(F_1 + F_2)$
R ( $C_s^d$ )	$45(R_1 + R_2)$
S ( $C_s^v$ )	$10(5S_1 + 4S_2)$
N ( $C_s^v$ )	$10(5N_1 + 4N_2)$
T ( $C_s^v$ )	$10(5T_1 + 4T_2)$

## CONCLUSIONS

By means of polarized Raman scattering and infrared reflection spectroscopy phonon excitations in hexagonal HoMnO<sub>3</sub> single crystals are studied. The zone-center vibrations are assigned to definite crystal modes based on their polarization properties and the results of the shell model lattice dynamics calculations. The results of the

group-theoretical analysis of the two-phonon processes and Raman scattering selection rules are used to interpret experimental second-order Raman scattering spectra. At the magnetic transition temperature  $T_N = 76\text{K}$  pronounced anomalies of the Raman- and infrared-active phonon modes, which modulate Mn-Mn interaction, are found experimentally and interpreted as the evidence for spin-phonon coupling.

This work is supported in part by the State of Texas through the Texas Center for Superconductivity and Advanced Materials at the University of Houston. MMG greatly acknowledges the support of the Bulgarian Science Found (Project F-1207).

- 
- [1] Smolenskii G A and Chupis I E 1982 *Sov. Phys. Usp.* **25** 475 [1982 *Usp. Fiz. Nauk* **136-138** 415].
  - [2] Huang Z J, Cao Y, Sun Y Y, Xue Y Y, and Chu C W 1997 *Phys. Rev. B* **56** 2623.
  - [3] Fröhlich D, Leute S, Pavlov V V, and Pisarev R V 1998 *Phys. Rev. Lett.* **81**, 3239.
  - [4] Iizuka-Sakano T, Hanamura E, and Tanabe Y 2001 *J. Phys: Condens. Matter* **13** 3031.
  - [5] Fiebig M, Lottermoser Th, Fröhlich D, Goltsev A V, and Pisarev R V 2002 *Nature* **419** 818.
  - [6] Fiebig M, Fröhlich D, Kohn K, Leute St, Lottermoser Th, Pavlov V V, and Pisarev R V 2000 *Phys. Rev. Lett.* **84** 5620.
  - [7] Muñoz A, Alonso J A, Martínez-Lope M J, Casáis M T, Martínez J L, and Fernández-Díaz M T 2001 *Chem. Mater.* **13** 1497.

- [8] Takahashi J, Hagita K, Kohn K, Tanabe Y, and Hanamura E 2002 *Phys. Rev. Lett.* **89** 076404.
- [9] Iliiev M N, Hadjiev V G, Litvinchuk A P, and Meng R L 2003 *Phys. Rev. Lett.* **90** 069701.
- [10] Sato T J, Lee S-H, Katsufuji T, Masaki M, Park S, Copley J R D, and Takagi H 2003 *Phys. Rev. B* **68** 014432 (2003).
- [11] Iliiev M N, Lee H-G, Popov V N, Abrashev M V, Hamed A, Meng R L, and Chu C W 1997 *Phys. Rev. B* **56** 2488.
- [12] Krytayakirana K, Berger P, and Jones R V, 1965 *Opt. Commun.* **1** 95.
- [13] Litvinchuk A P et al., unpublished results.
- [14] Souchkov A B, Simpson J R, Quijada M, Ishibashi H, Hur N, Ahn J S, Cheong S W, Millis A J, and Drew H D 2003 *Phys. Rev. Lett.* **91**, 027203.
- [15] Chen X K, Irwin J C, and Frank J P 1995 *Phys. Rev. B* **52** R13130.
- [16] Iliiev M N, Litvinchuk A P, Lee H-G, Chen C L, Dezaneti M L, and Chu C W 1999 *Phys. Rev. B* **59** 364.
- [17] Iliiev M N, Litvinchuk A P, Lee H-G, Chu C W, Barry A, and Coey J M D 1999 *Phys. Rev. B* **60** 33.
- [18] Yu T, Shen Z X, Sun W X, Lin J Y and Ding J 2003 *J. Phys.: Condens. Matter* **15** L213.
- [19] Burns G and Glazer A M 1993 *Space Groups for Solid State Scientists*, Academic Press, New York.
- [20] Gorban' I S and Lugovoi V I, 1976 *J. Appl. Spectr.* **24** 233 [1976 *Zh. Prikl. Spectr.* **24** 333].
- [21] Siegle H, Kaczmarczyk G, Filippidis L, Litvinchuk A P, Hoffmann A, and Thomsen C 1997 *Phys. Rev. B* **55** 7000.